

Precision Temperature Control of High-Throughput Fluid Flows: Theoretical and Experimental Analysis

Kevin M. Lawton

Steven R. Patterson

e-mail: spatters@unc.edu

Russell G. Keanini

Center for Precision Metrology,
Department of Mechanical Engineering and
Engineering Science,
University of North Carolina at Charlotte,
Charlotte, NC 28223

A precision method for attenuating temperature variations in a high-throughput control fluid stream is described and analyzed. In contrast to earlier investigations, the present study emphasizes heat transfer analysis of the constituent control device and derives theoretical descriptions of system responses to time-varying fluid temperatures. Experiments demonstrate that the technique provides: (1) frequency-dependent attenuation which is several orders of magnitude greater than that obtained via a perfect mixing volume; (2) attenuation, over two decades of disturbance frequency, that reduces in-flow temperature variations by factors ranging from 10 to $\approx 10^4$; (3) asymptotic attenuation greater than three orders of magnitude for spectral components having periods less than the device thermal equilibrium time; and (4) attenuation which is fully consistent with theoretical predictions. The model developed provides design criteria for tailoring system performance. In particular, it is shown that for a given control stream flow rate, the magnitude of maximal attenuation can be adjusted by varying the thermal resistance between the flow and attenuating medium, while the range of frequencies maximally attenuated can be adjusted by varying the product of thermal resistance and attenuating medium heat capacity. The analysis and design are general and should prove useful in the design and analysis of other high-throughput precision temperature control systems. [DOI: 10.1115/1.1375810]

Keywords: Control, Heat Transfer, Heat Exchangers

1 Introduction

Due to the inherent thermal sensitivity of materials and systems, precision experiments and instrumentation generally require precision temperature control. In some experiments, thermal effects can be the largest source of dimensional error and non-repeatability [1]. Likewise, thermal variability can limit the operation of various sensors and devices, e.g., laser interferometers, autocollimators, and capacitance probes [2]. Temperature stability, i.e., the maintenance of a given temperature to a given degree of precision, often constitutes a particularly challenging aspect of precision system design [3].

Precision temperature control near room temperature has received significant attention. One class of controllers uses resistive heaters to maintain a small enclosure near ambient. Due to the small size of these systems, high stability, on the order of $\pm 10 \mu\text{K}$ to $\pm 100 \mu\text{K}$ over hours, days or months of time can be achieved. Examples include $\pm 20 \mu\text{K}$ stability in standard cells over several months [4], $\pm 60 \mu\text{K}$ stability in laser diodes over approximately one hour [5], $\pm 10 \mu\text{K}$ stability in geophysical accelerometers over several days [6], and $\pm 100 \mu\text{K}$ stability in semiconductor lasers over tens of hours [7]. Resistance-based controllers providing milliKelvin stability have also been developed or proposed for use in thermometry [8], physical property measurement [9,10], strain measurement [9], and optical microscopy [11].

Another class of controllers uses fluids to heat or cool enclosures near room temperature. Since these controllers have both heating and cooling capabilities, they are particularly suited for use with heat-generating devices. Examples include an oil-cooled

vacuum chamber providing $\pm 15 \mu\text{K}$ control over tens of hours [12], precision temperature-controlled water baths providing $\pm 25 \mu\text{K}$ stability over tens of hours [13,14], and a stirred water bath providing $\pm 3.5 \mu\text{K}$ stability over tens of hours [15].

In contrast to resistance-based precision thermal control and precision thermal control in closed, non-circulating fluid systems, relatively little work has been reported on precision thermal control of flowing or recirculating control fluid streams. Lopez and Barron [16] used temperature-controlled forced air to achieve $\pm 0.1 \text{ K}$ control over liquid crystal samples. Ogasawara [14] used recirculating water to maintain a thermostatic water bath to within $\pm 25 \mu\text{K}$ of a set point. This approach had also been used to control plasma tube temperatures in lasers [17,18]. Sydenham and Collins [19], using recirculating water in a deep underground test facility (where the latter minimized background thermal variations), achieved $\pm 40 \mu\text{K}$ stability in a 10 m long steel standard over hundreds of hours.

This paper describes the theoretical models, design, construction, and performance of a "thermal gradient attenuator" low-pass filter. This device is a critical component for producing a high stability chilled water supply that can be used for precision temperature control. By attenuating higher frequency temperature oscillations in the control fluid, active heater controllers need only reject lower frequency disturbances to achieve precise temperature control.

This work extends previous investigations by developing a relatively simple approach capable of providing centiKelvin stability over hours and milliKelvin stability over minutes, within recirculating flows. Equally important, considerable attention is devoted to modeling system heat transfer and system dynamics.

Contributed by the Heat Transfer Division for publication in the JOURNAL OF HEAT TRANSFER. Manuscript received by the Heat Transfer Division June 27, 2000; revision received January 20, 2001. Associate Editor: D. A. Zumbrennen.

2 Thermal Gradient Attenuator—Justification for Need

A multi-purpose temperature-controlled chamber has been designed for use in precision metrology experiments. The chamber walls are channeled to allow flow of temperature-controlled chilled water, which in turn provides thermal control of the chamber interior. Although a heater controller is available to modulate the chilled water temperature, because of limited bandwidth it cannot reject the higher frequency temperature oscillations of the available chilled water supply (see Figs. 1 and 2). Since the desired level of temperature control is order 0.1 mK, the large short-term temperature deviations of the chilled water must be significantly attenuated before entering the heater control system.

In order to attenuate these higher frequency oscillations, a thermal gradient attenuator, shown schematically in Fig. 3, must be placed in the chilled water stream. As shown in Figs. 1 and 2, the spectrum for the entering chilled water stream contains significant spectral components over the range from 0.04 to 10 mHz, with peak rates of change of order 1 K/min. With dominant temporal variations occurring at relatively low frequencies, effective attenuation requires that the attenuator exhibit large attenuation at the relatively low frequency of 0.04 mHz.

For the purpose of analysis, the thermal gradient attenuator is modeled as three subsystems, each characterized by a dominant heat transfer mode and an associated dynamic. The core of the device is identified as the tube bank-attenuator subsystem since it consists of an array of uniformly distributed identical tubes that direct the flow of the control fluid past the attenuator medium. The entrance and exit volumes below and above the tube bank-attenuator are identified as the lower accumulator and upper accumulator subsystems. Subsystem and total device performance are characterized using transfer functions, which model the ratio of the output and input temperatures as functions of frequency.

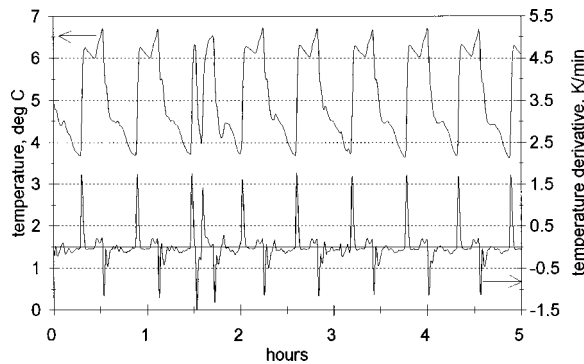


Fig. 1 Chilled water temperature and temperature derivative versus time, 1.9 l/min flow rate

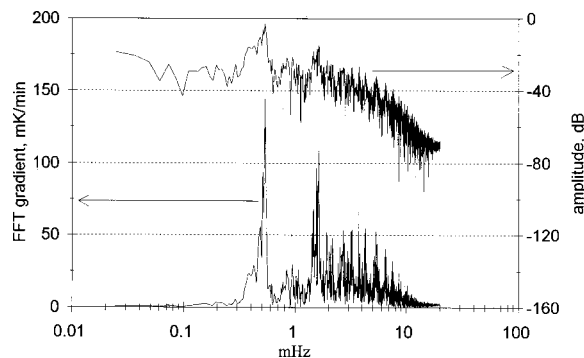


Fig. 2 Chilled water spectrum and average FFT gradients versus frequency; 1.9 l/min flow rate

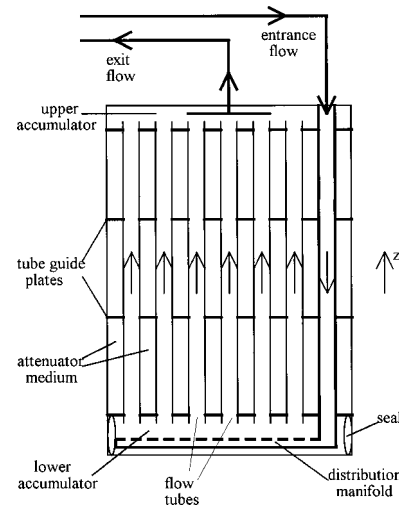


Fig. 3 Thermal gradient attenuator configuration

3 Lumped-Differential Model of the Tube Bank-Attenuator Subsystem

The model of the tube bank-attenuator sub-system is based on two radially-lumped, coupled differential equations which model the time and axially-dependent temperature variations within the flowing control fluid and the surrounding attenuating medium. The derivation of these equations proceeds in three steps: (1) assumptions relevant to the tube bank-attenuator are stated; (2) order of magnitude arguments are used to simplify the energy equation within the flow, the tube wall, and the surrounding attenuating medium; and (3) each simplified equation is radially integrated, leading to the lumped working equations. Neto and Cotta [20,21] have developed a lumped-differential analysis of double-pipe heat exchangers. The present formulation for a restricted class of heat exchanger leads to two relatively simple, integrable differential equations, while the more general approach in Neto and Cotta, which incorporates a generalized integral transform method [22], leads to a large system of coupled differential equations.

The class of heat exchangers modeled here is restricted by a set of assumptions relating to the geometry, thermal properties of the components, and the frequency range of the input disturbances. These assumptions can be related to a single tube and the surrounding attenuator medium. The length of the attenuator medium is taken to be much larger than the radial dimension, and the ratio of axial fluctuation length scale, \bar{w}/f , to radius, r , is sufficiently small that radial conduction dominates axial conduction. Thus,

$$\frac{\bar{w}/f}{r} \gg 1 \quad \text{so that} \quad \frac{\partial T}{\partial r} \gg \frac{\partial T}{\partial z} \quad (1)$$

and

$$r/L \ll 1. \quad (2)$$

It is also assumed that the attenuator medium is either a solid or a stagnant fluid where advection is negligible. In the latter case, it is assumed that the ratio of conductive to time-dependent temperature variations

$$\frac{\vec{u} \cdot \nabla T}{\partial T / \partial t} \approx \frac{u_s}{f \cdot L} \quad (3)$$

are small, where the velocity scale, $u_s = (g \cdot \beta \cdot L \cdot \Delta T)^{1/2}$, is determined by buoyancy.

Based on these assumptions, heat transfer, to first order, within the attenuator medium is governed by the equation

$$\frac{\partial T}{\partial t} = \alpha_a \frac{1}{r} \cdot \frac{\partial}{\partial r} \left(r \frac{\partial T}{\partial r} \right). \quad (4)$$

Similarly, conduction within the tube wall is governed by

$$\frac{\partial}{\partial r} \left(r \frac{\partial T}{\partial r} \right) = 0 \quad (5)$$

while within the fluid flow

$$\frac{\partial T}{\partial t} + w(r) \frac{\partial T}{\partial z} = \alpha_a \frac{1}{r} \cdot \frac{\partial}{\partial r} \left(r \frac{\partial T}{\partial r} \right), \quad (6)$$

where $w(r)$ is the fully-developed laminar flow velocity profile [23]. For tubes with sufficiently high aspect ratio and small Reynolds number, the entry length comprises a small fraction of the total length, and the above equation is a good approximation for the entire tube.

Equations (4) through (6) may be integrated radially to obtain respective lumped equations for the mean temperature in the attenuator, tube wall, and fluid flow regions

$$\frac{\partial \bar{T}_a}{\partial t} = \frac{\alpha_a}{(r_a - r_i)^2} \left(r_a \frac{\partial T}{\partial r} \Big|_{r_a} - r_i \frac{\partial T}{\partial r} \Big|_{r_i} \right) \quad (7)$$

$$r_f \frac{\partial T}{\partial r} \Big|_{r_f} = r_i \frac{\partial T}{\partial r} \Big|_{r_i} \quad (8)$$

$$\frac{\partial \bar{T}_f}{\partial t} + \frac{1}{r_f^2} \int_0^{r_f} r w(r) \frac{\partial T}{\partial z} dr = \frac{\alpha}{r_f} \frac{\partial T}{\partial r} \Big|_{r_f}, \quad (9)$$

where the mean temperatures are defined as

$$\bar{T}_a(z, t) = \frac{1}{r_a^2 - r_i^2} \int_{r_i}^{r_a} r \cdot T(r, z, t) \cdot dr \quad (10)$$

$$\bar{T}_f(z, t) = \frac{1}{r_f^2} \int_0^{r_f} r \cdot T(r, z, t) \cdot dr. \quad (11)$$

When the radial conduction time scale is much shorter than the disturbance and axial convection time scales, radial temperature gradients are quickly smoothed, and the integral in Eq. (9) may be approximated as

$$\int_0^{r_f} r w(r) \frac{\partial T}{\partial z} dr \approx r_f^2 \bar{w} \frac{\partial \bar{T}_f}{\partial z}, \quad (12)$$

where the radially averaged velocity is given by

$$\bar{w} = \frac{2}{r_f^2} \int_0^{r_f} r w(r) dr. \quad (13)$$

The integrated energy equation, Eq. (8), implies that at any instant, the local radial heat transfer rate, $q = q(z, t)$, is constant within the tube wall. By solving Eq. (5), it is readily shown that

$$q(z, t) = 2 \pi k_t L \frac{[T(r_f, z, t) - T(r_i, z, t)]}{\ln(r_i/r_f)} = \frac{[T(r_f, z, t) - T(r_i, z, t)]}{R_t} \equiv \frac{[T|_{r_f} - T|_{r_i}]}{R_t}, \quad (14)$$

where R_t is the total tube thermal resistance along its length, L . Similarly, heat transfer at the inner and outer tube boundaries are given as

$$q(z, t) = \frac{[\bar{T}_f - T|_{r_f}]}{R_f} = -r_f k_f L \frac{\partial T}{\partial r} \Big|_{r_f}, \quad (15)$$

where R_f is the fluid thermal resistance, and

$$q(z, t) = \frac{[T|_{r_i} - \bar{T}_a]}{R_a}, \quad (16)$$

where R_a is the attenuator thermal resistance. Given the following definition and equation

$$R \equiv R_f + R_t + R_a = \frac{[\bar{T}_f - T|_{r_f}]}{q} + \frac{[T|_{r_f} - T|_{r_i}]}{q} + \frac{[T|_{r_i} - \bar{T}_a]}{q} = \frac{[\bar{T}_f - \bar{T}_a]}{q} \quad (17)$$

and substituting Eqs. (13) and (15) into Eq. (9) yields

$$\frac{\partial \bar{T}_f}{\partial t} + \bar{w} \frac{\partial \bar{T}_f}{\partial z} = \frac{1}{\tau_f} (\bar{T}_a - \bar{T}_f), \quad (18)$$

where $\tau_f = RC_f$ is the fluid time constant. Similarly, Eq. (7) simplifies to

$$\frac{\partial \bar{T}_a}{\partial t} = \frac{1}{\tau_a} (\bar{T}_f - \bar{T}_a), \quad (19)$$

where $\tau_a = RC_a$, is the attenuator time constant.

4 Tube Bank-Attenuator Transfer Function

Neglecting heat transfer through the outer wall of the attenuator assembly, the transfer function of the entire tube bank-attenuator is the same as that of a single tube, given proper flow rate scaling. Thus, the transfer function of the entire tube bank follows from Eqs. (18) and (19). A more compact result follows by introducing the dimensionless space and time variables

$$\eta = z/(\bar{w} \tau_a) \quad \text{and} \quad \tau = t/\tau_a \quad (20)$$

and the dimensionless heat capacity ratio

$$\zeta = \tau_a / \tau_f = C_a / C_f. \quad (21)$$

Substitution of Eqs. (20) and (21) into Eqs. (18) and (19) yields

$$\frac{\partial \bar{T}_f}{\partial \tau} + \frac{\partial \bar{T}_f}{\partial \eta} = \zeta (\bar{T}_a - \bar{T}_f) \quad (22)$$

$$\frac{\partial \bar{T}_a}{\partial \tau} = (\bar{T}_f - \bar{T}_a). \quad (23)$$

Taking the Laplace transforms of Eqs. (22) and (23), with initial conditions equal to zero, yields

$$s \hat{T}_f + \frac{\partial \hat{T}_f}{\partial \eta} = \zeta (\hat{T}_a - \hat{T}_f) \quad (24)$$

$$s \hat{T}_a = (\hat{T}_f - \hat{T}_a), \quad (25)$$

where $s = 2i\pi f \tau_a$, and f is the frequency in Hz. Eliminating \hat{T}_a yields

$$\frac{\partial \hat{T}_f}{\partial \eta} + \frac{s}{s+1} (s + \zeta + 1) \hat{T}_f = 0. \quad (26)$$

This equation is readily solved to provide an expression for the fluid temperature as a function of dimensionless length and dimensionless frequency

$$\hat{T}_f(\eta, s) = \hat{T}_f(\eta=0, s) \cdot \exp \left[\frac{-s}{s+1} (s + \zeta + 1) \eta \right]. \quad (27)$$

Thus, the tube bank transfer function [24] is given by

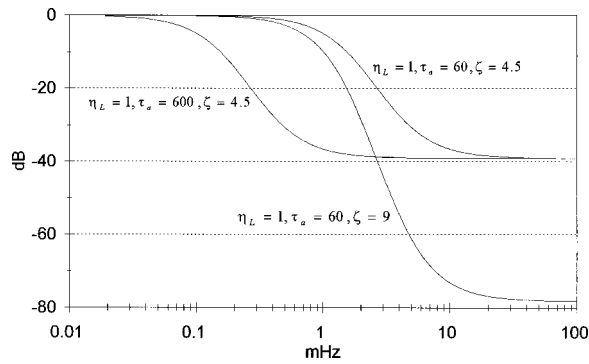


Fig. 4 Theoretical model transfer functions versus frequency

$$\begin{aligned} Trm_a(s) &= \frac{\hat{T}_f(\eta = \eta_L, s)}{\hat{T}_f(\eta = 0, s)} = \exp\left[\frac{-s}{s+1}(s + \zeta + 1)\eta_L\right] \\ &= \exp\left[\frac{-s \cdot \zeta \cdot \eta_L}{s+1}\right] \cdot \exp[-s \cdot \eta_L], \end{aligned} \quad (28)$$

where the latter form separates the effect of transport delay, $\exp(-s \cdot \eta_L)$, from other effects in the attenuator. Since only the real part of the exponent affects the magnitude of the transfer function, the transfer function magnitude can be expressed in the form

$$Trm_a(s) = \exp\left[-\zeta \cdot \eta_L \cdot \text{Re}\left(\frac{s}{s+1}\right)\right]. \quad (29)$$

Figure 4 depicts the tube bank-attenuator transfer function for several values of η_L , ζ , and τ_a . For a given dimensionless length, η_L , the heat capacity ratio, ζ , determines the magnitude of the asymptotic attenuation. In addition, for a given η_L , the range of frequencies optimally attenuated increases as τ_a increases, so that attenuation extends to lower disturbance frequencies. In particular, the asymptotic attenuation is proportional to

$$\zeta \cdot \eta_L = \frac{C_a}{C_f} \frac{L}{2\bar{w}\tau_a} = \frac{1}{\dot{m}c_f R}, \quad (30)$$

which means that given a fluid with mass flow rate, \dot{m} , and specific heat, c_f , the total thermal resistance between the fluid flow and the attenuator medium determines the asymptotic attenuation. In terms of dimensional variables, the transfer function, Eq. (29), is

$$Trm_a(f) = \exp\left[-\frac{1}{\dot{m}c_f R} \cdot \text{Re}\left(\frac{2i\pi f\tau_a}{2i\pi f\tau_a + 1}\right)\right]. \quad (31)$$

This form more clearly shows the effect of τ_a in determining the frequency at which significant attenuation occurs. Given a thermal resistance to achieve an asymptotic attenuation requirement, the heat capacity of the attenuator, C_a , determines the attenuator time constant, which in turn determines the frequency range over which asymptotic attenuation is closely approached.

5 Tube Bank-Attenuator Configuration and Properties

In order to efficiently package a large heat capacity (to attenuate a wide range of frequencies), the attenuator medium should have large specific heat capacity (heat capacity per volume). Other considerations for the medium include cost and ease of distributing the material about the tubes in order to provide the desired thermal resistance for optimal attenuation. Water fulfills these requirements well since it is inexpensive and has a specific capacity

(4.2 MJ K⁻¹ m⁻³) which is higher than that of aluminum, steel, copper, and numerous other, more expensive materials.

The device configuration consists of an externally insulated 208 liter (55-gallon) drum, 947 nylon tubes (each 0.8 m long and 4.8 mm in diameter), and 4 acrylic spacer plates (Fig. 3). Chilled water enters the attenuator from the top, flows to the bottom where it is distributed to the tube bank through a lower accumulator, flows upward through the tubes into an upper accumulator, and then exits. Nylon was chosen as the tube material because of its low cost and suitable thermal resistance. The tubes are arranged in a hexagonal pattern with tube center spacing of approximately 16 mm. Thus, each tube is surrounded by an annulus of attenuator medium having an effective radius of approximately 8 mm. The tube aspect ratio condition of Eq. (2) is satisfied for this configuration since $r/L = O(10^{-2})$. Also, the radially lumped model is valid for frequencies below an upper frequency limit determined by the inverse of the radial diffusion time scale

$$f_1 \approx \frac{\alpha_a}{(r_m)^2} = O(10^{-2} \text{ Hz}), \quad (32)$$

where r_m is the radius encompassing half of the area of the attenuator medium.

Because the in-tube temperature variations are small relative to the dominant input temperature variations, the tube wall is approximately isothermal. Thus, the convection coefficient can be computed from the laminar, thermally fully developed flow condition [25]

$$h_f = \text{Nu} \frac{k_f}{D_f} = 3.66 \frac{k_f}{D_f}. \quad (33)$$

Given h_f , the fluid thermal resistance is

$$R_f = \frac{1}{h_f A_s}, \quad (34)$$

where A_s is the convection surface area. The validity of the assumption of thermally fully developed flow is supported by the fact that the thermal development length [23] for these parameters is approximately 2 percent of the tube length.

The attenuator thermal resistance, R_a , is based on the approximation of steady state conduction through a stationary fluid. From Eqs. (3) and (32), the ratio of the time derivative to radial diffusion terms is small, so that the temperature field is approximately steady within the attenuator medium. Thus, the effective attenuator thermal resistance is

$$R_a = \frac{\ln(r_m/r_i)}{2\pi k_a L}. \quad (35)$$

6 Accumulator and Total Transfer Functions

In order to complete the model of the entire device, the transfer functions of the upper and lower accumulators must be developed. Chilled water is distributed to the tube bank by the lower accumulator and collects prior to exiting in the upper accumulator. The lower accumulator feeds the tube bank through a perforated-tube distribution manifold containing numerous small holes (Fig. 3). The flow through each hole produces a small jet within the lower accumulator, which in turn, induces strong mixing. It is thus assumed that the lower accumulator functions as a perfectly mixed volume, with the corresponding lumped energy equation given by

$$\rho_f \frac{d\bar{T}_{la}}{dt} V_{la} = \dot{M}(T_{in}(t) - \bar{T}_{la}), \quad (36)$$

where \dot{M} is the total mass flow rate for all of the tubes, $T_{in}(t)$ is the time varying input temperature, V_{la} is the lower accumulator volume, and \bar{T}_{la} is the average lower accumulator temperature. Taking the Laplace transform yields the transfer function

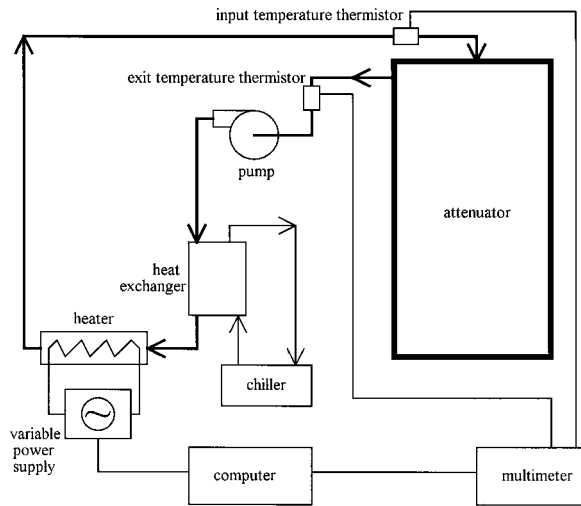


Fig. 5 Attenuator test setup

$$Tr_{la}(s) = \frac{1}{1 + \tau_m s}, \quad (37)$$

where $\tau_m = \rho_f V_{la} / \dot{M}$ is the characteristic residence time for the flow in the lower accumulator.

In contrast to the lower accumulator, mixing in the upper accumulator is relatively weak. In addition, since the length, L_{ua} , of the upper accumulator is much smaller than the radius, r_{ua} , axial conduction dominates the heat transfer. Considering the scales of each term in the associated energy equation, and assuming that the flow is essentially vertical and uniform across the upper accumulator, the governing equation is

$$\frac{dT_{ua}}{dt} + \bar{w}_{ua} \frac{dT_{ua}}{dz} = \alpha_f \frac{d^2 T_{ua}}{dz^2}, \quad (38)$$

where \bar{w}_{ua} is the uniform vertical velocity across the accumulator. Taking the Laplace transform of Eq. (38), the associated transfer function is

$$Tr_{ua}(s) = \exp(\lambda L_{ua}), \quad (39)$$

where $\lambda = (\bar{w}_{ua} - \sqrt{\bar{w}_{ua}^2 + 4\alpha_f^2}) / 2\alpha_f$. Given Eqs. (28), (37), and (39), the total transfer function of the entire attenuator device is

$$Tr_T(s) = Tr_{la}(s) \cdot Tr_a(s) \cdot Tr_{ua}(s). \quad (40)$$

7 Experimental Setup

An experimental setup for testing attenuator performance is shown in Fig. 5. A constant-displacement pump maintains a constant flow rate of water through the system. A cartridge heater, controlled through a computer-based data acquisition board and connected to a variable power supply, is used to impose single-frequency sinusoidal temperature variations on the flow. The computer also captures input and output temperatures from the thermal gradient attenuator using thermistors and a high-precision digital multimeter (via GPIB interface).

8 Transfer Function Results

Measured and theoretical transfer functions for the thermal gradient attenuator are shown in Fig. 6, where attenuation is shown for 18 imposed frequencies. The root mean squared (RMS) difference between measured and theoretical values is approximately 3 dB. Also shown for reference is a transfer function corresponding to a perfectly mixed attenuator volume and a transfer function corresponding to an attenuator dominated by axial conduction, where the total volume is equal to that of the experimental device.

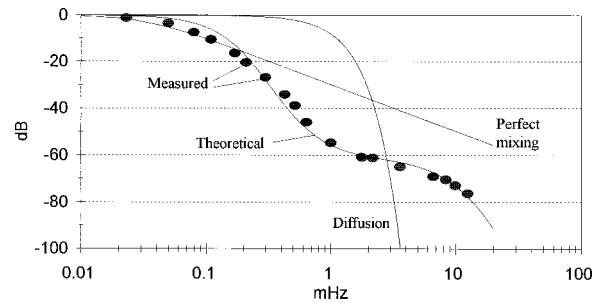


Fig. 6 Drum attenuator transfer functions versus frequency; measured, theoretical, perfect mixing, and diffusion for 2.5 l/min flow rate

In the region near 1 mHz, where time derivatives of temperature are largest (and are thus least conducive to precision thermal control), the attenuator provides in excess of 20 dB more attenuation than a perfect mixer. Likewise, in the lower portion of the frequency range, $f < 3$ mHz, the attenuator provides significantly more attenuation than does axial diffusion. Although axial diffusion provides more attenuation for $f > 3$ mHz, this occurs beyond the point where the attenuator has already provided 60 dB of attenuation.

Attenuator performance compares favorably with that obtained by Ogasawara [14]. Ogasawara's device consisted of a fluid-filled enclosure in which spiral baffles promoted mixing of water. He reported that the device reduced temperature variations by a factor of 3. By contrast, and as shown in Fig. 6, the thermal gradient attenuator provides attenuation on the order of 60 dB, corresponding to factor of reduction on the order of 10^3 . Interestingly, it appears that Ogasawara's device can be modeled as a perfectly mixed volume; indeed, the order of attenuation obtained by Ogasawara is consistent with the degree of attenuation associated with a perfect mixer.

Four additional sets of attenuation data are shown in Fig. 7, with standard measurement [26] and model uncertainties. Each data set, corresponding to a different chilled water flow rate, was obtained following a minor device modification (where a seal was installed to eliminate small leaks between the tube bank and the lower accumulator). Consistent with the results shown in Fig. 6, the measurements in Fig. 7 match theoretical predictions to within 5 dB RMS. The largest discrepancies appear at very low frequencies where chilled water input temperature variations are small and large attenuation is not needed. The theoretical envelopes representing model uncertainty are calculated via Eq. (40) using measured mean flow rates and mean attenuator water levels along

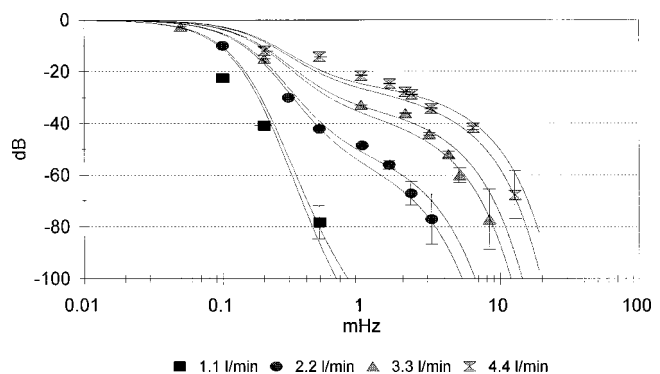


Fig. 7 Measured and theoretical transfer functions versus frequency, with uncertainty bars on measured points and uncertainty envelopes for theoretical curves, where envelopes reflect uncertainty in flow rates and accumulator water levels

with associated estimated uncertainties. Measurement uncertainty is estimated by first expressing the system transfer function as the ratio of the amplitudes of the output and input temperature variations

$$Tr(f) = \frac{T_{out}(f)}{T_{in}(f)}. \quad (41)$$

The uncertainty in the transfer function is then estimated by assuming that individual uncertainties are independent and normally distributed, so that [27]

$$\sigma_{Tr} = \left[\left(\frac{\partial Tr}{\partial T_{out}} \right)^2 \cdot \sigma_{T_{out}}^2 + \left(\frac{\partial Tr}{\partial T_{in}} \right)^2 \cdot \sigma_{T_{in}}^2 \right]^{1/2}, \quad (42)$$

where

$$\sigma_{T_{out}}^2 = \sigma_{T_{out}}^2(f) = (S_t \cdot \sigma_T)^2 + (T_{out}(f) \cdot \sigma_s)^2 \quad (43)$$

$$\sigma_{T_{in}}^2 = \sigma_{T_{in}}^2(f) = (S_t \cdot \sigma_T)^2 + (T_{in}(f) \cdot \sigma_s)^2 \quad (44)$$

and σ_T ($=0.25$ ohm) is the thermistor measurement uncertainty, S_t ($=1.77 \cdot 10^{-3}$ K/ohm) is the nominal thermistor sensitivity, and σ_s ($=5 \cdot 10^{-4}$ K/K) is the uncertainty of S_t .

9 Attenuation of Broadband Thermal Variations

The device performance was also tested with the inlet stream subject to broadband thermal disturbances. For this experiment, in-house chilled water serves as the control fluid stream, where the associated power spectrum in Fig. 2 shows that temperature variations are spectrally broadband. In addition, a sinusoidal (8.6 mHz) thermal variation was superimposed on the control fluid stream to provide additional higher frequency disturbance to fully test the attenuator performance (at 2.2 l/min flow rate). As shown in Fig. 8, the resultant in-stream temperature exhibits large amplitude (3.5 K peak to peak) variations and equally large (4 K/min) time rates of change.

Under these conditions, the device functions as a low-pass filter, where high frequency disturbances are suppressed to magnitudes below measurement sensitivity (for the 8.6 mHz variation), and transmitted low frequency disturbances are reduced in magnitude; see Fig. 9. The dominant variation in the output stream reflects the slow periodic oscillation of the input at approximately 3 cycles every 2 hours (≈ 0.4 mHz). The attenuation of approximately 2 orders of magnitude for this low frequency (Fig. 7) is consistent with the data in Figs. 8 and 9.

The most important result of Fig. 9 is the dramatic reduction in the short-term variations, or temperature derivative. Achieving temperature control better than milliKelvin levels without filtering the input stream in Fig. 8 would be very difficult because of the large and rapidly changing disturbances. After attenuation by the attenuator device, the short-term deviations are reduced by 3 or-

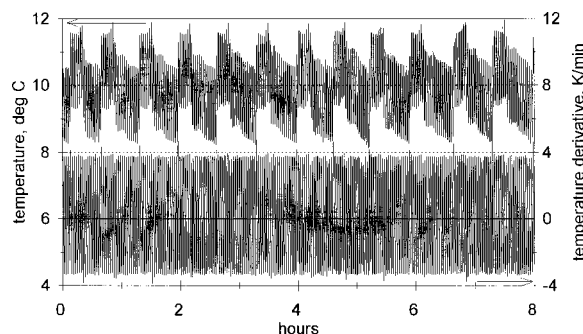


Fig. 8 Attenuator input temperature and temperature derivative versus time for an unfiltered chilled water stream with a superimposed 8.6 mHz sinusoid

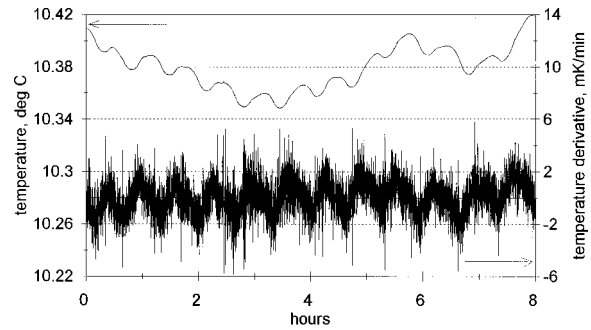


Fig. 9 Attenuator output temperature and temperature derivative versus time for the unfiltered chilled water stream with a superimposed 8.6 mHz sinusoid

ders of magnitude to order 1 mK/min, which is a suitably well behaved source for precision temperature control.

10 Summary and Conclusions

The analysis, design, and performance of a precision thermal gradient attenuator has been presented. For purposes of analysis, the system was decomposed into three subsystems: a lower accumulator where the control fluid collects and is passively mixed, a tube bank-attenuator where the control fluid exchanges heat with a surrounding, stagnant attenuation medium (here, water), and an upper accumulator where the control fluid again collects prior to exiting the device. Analytic expressions have been developed to describe the performance of each subsystem and the total system.

A set of experiments in which sinusoidal temperature disturbances are imposed on the control fluid stream, have been performed in order to evaluate device performance. Performance measured over a disturbance frequency range from 0.1 mHz to 10 mHz, and at four representative control stream flow rates, is well described by the analytic model. At all but the lowest frequencies, the system provides significantly greater attenuation than that produced by a perfectly mixed volume. In addition, a comparison with earlier work [14] shows that the present device provides frequency-dependent attenuation which is two, and, at higher frequencies, almost three orders of magnitude greater than the earlier device.

Finally, an experiment was performed to investigate the system performance under conditions where the control stream is subject to broadband thermal disturbances. In this case, the system functions as a low-pass filter/attenuator, effectively eliminating spectral components having periods shorter than the device thermal equilibration time, τ_d , and attenuating lower frequency components. Consistent with attenuation observed for spectrally pure disturbances, it is found that unfiltered temperature oscillations exhibit increasing attenuation with increasing spectral frequency.

The analytic model allows prediction of system response and provides simple criteria for designing system performance. The model shows that for fixed control stream flow rate, the magnitude of maximal attenuation can be tuned by adjusting the total thermal resistance between the stream and the attenuator medium. Given a thermal resistance that produces a desired maximal attenuation, the frequency range subject to maximal attenuation can be tuned by adjusting the attenuator heat capacity. The analysis and design are general and should prove useful in the design and analysis of other high-throughput precision temperature control systems.

Acknowledgment

This work was supported by the National Science Foundation, Grant No. DMI-9500390.

Nomenclature

α_a, α_f	= attenuator and fluid diffusivities
A_s	= convection surface area
β	= thermal expansion coefficient
C_a, C_f	= single tube attenuator and fluid total heat capacities
D_f	= fluid diameter
f	= frequency, Hz
f_l	= upper frequency limit determined by the inverse radial diffusion time scale
h_f	= fluid convection coefficient
k_a, k_f, k_t	= attenuator, fluid, and tube conductivities l/min
L	= attenuator tube length
L_{ua}	= upper accumulator length
\dot{m}	= mass flow rate of water through each tube
\dot{M}	= total mass flow rate of water through the attenuator device
η	= dimensionless axial coordinate
η_L	= dimensionless tube length
$O()$	= order of magnitude of the expression
ρ_f	= fluid density
r_a, r_f, r_t	= attenuator, fluid and tube outer radii
r_m	= radius encompassing half of the attenuator area
r_{ua}	= upper accumulator outer radius
R	= thermal resistance between the fluid flow and the lumped attenuator medium
R_a, R_f, R_t	= attenuator, fluid, and tube thermal resistances
s	= dimensionless Laplace transform variable
τ	= dimensionless time
τ_a, τ_f	= attenuator and fluid time constants
τ_m	= characteristic residence time for the flow in the lower accumulator
T	= temperature
\bar{T}_a, \bar{T}_f	= radially averaged mean attenuator and fluid temperatures
\hat{T}_a, \hat{T}_f	= Laplace transformed mean attenuator and fluid temperatures
T_{in}, T_{out}	= time varying input and output temperatures
\bar{T}_{la}	= lower accumulator average temperature
Tr	= transfer function
$Tr_a, Tr_{la}, Tr_{ua}, Tr_T$	= attenuator, lower accumulator, upper accumulator, and total transfer functions
Trm_a	= attenuator transform function magnitude
$u_{\frac{z}{2}}$	= buoyancy velocity scale
\mathbf{u}	= vector velocity field
V_{la}	= volume of lower accumulator
w	= axial velocity in the z -direction

\bar{w}	= average axial in-tube fluid velocity
\bar{w}_{ua}	= average axial velocity in the upper accumulator
ζ	= heat capacity ratio: attenuator to fluid

References

- [1] Bryan, J., 1990, "International Status of Thermal Error Research," *Annals of the CIRP*, **39**, pp. 645–656.
- [2] Slocum, A. H., 1992, *Precision Machine Design*, Prentice Hall, NJ, p. 96.
- [3] Smith, S. T., and Chetwynd, D. G., 1997, *Foundations of Ultraprecision Mechanism Design*, Gordon and Breach, Amsterdam, p. 84.
- [4] Cutkosky, R. D., and Field, B. F., 1974, "Standard Cell Enclosure with 20 μ K Stability," *IEEE Trans. Instrum. Meas.*, **23**, pp. 295–298.
- [5] Lee, H. S., Yang, S. H., and Chung, N. S., 1990, "Temperature Controller Using an Error Signal Modulation," *Rev. Sci. Instrum.*, **61**, pp. 1329–1331.
- [6] Dratler, J., 1974, "A Proportional Thermostat with 10 Microdegree Stability," *Rev. Sci. Instrum.*, **45**, pp. 1435–1444.
- [7] Esman, R. D., and Rode, D. L., 1983, "100 μ K Temperature Controller," *Rev. Sci. Instrum.*, **54**, pp. 1368–1370.
- [8] Cutkosky, R. D., and Davis, R. S., 1981, "Simple Control Circuit for Temperature Control and Other Bridge Applications," *Rev. Sci. Instrum.*, **52**, pp. 1403–1405.
- [9] Strem, R. B., Das, B. K., and Greer, S. C., 1981, "Digital Temperature Control and Measurement System," *Rev. Sci. Instrum.*, **52**, pp. 1705–1708.
- [10] Williams, G. I., and House, W. A., 1981, "Thermistor Controlled Water/Oil Bath for Precision Measurements in the Range 0–30 C," *J. Phys. E*, **14**, pp. 755–760.
- [11] Miller, R. J., and Gleeson, H. F., 1994, "A Computer Interfaced High-Stability Temperature Controller and Heating Stage for Optical Microscopy," *Measurement Science and Technology*, **14**, pp. 904–911.
- [12] Sarid, D., and Cannell, D. S., 1974, "A 15 Microdegree Temperature Controller," *Rev. Sci. Instrum.*, **45**, pp. 1082–1089.
- [13] Harvey, M. E., 1968, "Precision Temperature-Controlled Water Bath," *Rev. Sci. Instrum.*, **39**, pp. 13–18.
- [14] Ogasawara, H., 1986, "Method of Precision Temperature Control Using Flowing Water," *Rev. Sci. Instrum.*, **57**, pp. 3048–3052.
- [15] Priel, Z., 1978, "Thermostat with a Stability of 3.5 μ K," *J. Phys. E*, **11**, pp. 27–30.
- [16] Iglesias, M. C. L., and Baron, M., 1990, "Temperature Control in Small Air-Heated Measuring Cells," *Rev. Sci. Instrum.*, **61**, pp. 2245–2246.
- [17] Ogasawara, H., and Nishimura, J., 1982, "Frequency Stabilization of Internal-Mirror He-Ne Lasers by a Flowing Water Method," *Appl. Opt.*, **21**, pp. 1156–1157.
- [18] Ogasawara, H., and Nishimura, J., 1983, "Frequency Stabilization of Internal-Mirror He-Ne Lasers," *Appl. Opt.*, **22**, pp. 655–657.
- [19] Sydenham, P. H., and Collins, G. C., 1975, "Thermistor Controller with Microkelvin Stability," *J. Phys. E*, **8**, pp. 311–315.
- [20] Neto, F. S., and Cotta, R. M., 1992, "Counterflow Double-Pipe Heat Exchanger Analysis Using a Mixed Lumped-Differential Formulation," *Int. J. Heat Mass Transf.*, **35**, pp. 1723–1731.
- [21] Neto, F. S., and Cotta, R. M., 1993, "Dynamic Analysis of Double-Pipe Heat Exchangers Subjected to Periodic Inlet Temperature Disturbances," *Warme and Stoffubertragung*, **18**, pp. 497–503.
- [22] Ozisik, M. N., and Murray, R. L., 1974, "On the Solution of Linear Diffusion Problems With Variable Boundary Conditions," *ASME J. Heat Transfer*, **96**, pp. 48–51.
- [23] Incropera, F., and DeWitt, D., 1990, *Introduction to Heat Transfer*, Wiley, New York, p. 432.
- [24] Dorf, R. C., and Bishop, R. H., 1995, *Modern Control Systems*, Addison-Wesley, New York, p. 394.
- [25] Bejan, A., 1984, *Convection Heat Transfer*, Wiley, New York, p. 298.
- [26] International Organization for Standardization, 1993, *Guide to the Expression of Uncertainty in Measurements*, Geneva.
- [27] Beckwith, T. G., Marangoni, R. D., and Lienhard, J. H., 1993, *Mechanical Measurements*, Addison-Wesley, New York, p. 82.